Electronic states in strained cleaved-edge-overgrowth quantum wires and quantum dots

M. Grundmann, O. Stier, and D. Bimberg
Institut für Festkörperphysik, Technische Universität Berlin, Hardenbergstrasse 36, D-10623 Berlin, Germany
(Received 11 March 1998)

The electronic properties of cleaved-edge-overgrowth (CEO) strained T-shaped quantum wires and twofold CEO quantum dots are calculated in the presence of strain induced by lattice mismatch. Potential modifications of growth morphology due to strain are discussed. The anisotropy of the elastic constants causes the band edges in (001) and (110)-oriented layers to be different. Using effective-mass theory, we find electrons to be localized in asymmetric strained T-shaped quantum wires, whereas holes are repelled. Coulomb interaction can induce localization of excitons. For twofold CEO quantum dots, bound states are expected only when (compressive) strain effects are small. In our calculation image charge effects are properly taken into account. Numerical examples are presented for the $In_{0.2}Ga_{0.8}As/GaAs$ system.
[S0163-1829(98)04339-2]

I. INTRODUCTION

Creation of nanostructures by cleaved-edge overgrowth (CEO) (Ref. 1) has generated considerable interest in recent years. T-shaped quantum wires (QWR's) at the juncture of two (unstrained) quantum wells (QWL's) made from $GaAs/Al_xGa_{1-x}As$ have been experimentally proven to provide bound states for charge carriers.[2,3] The electronic structure of these systems has been modeled in a number of papers in the effective-mass approximation[4] or employing $k\cdot p$ theory.[5,6] Excitonic effects were included in Refs. 7 and 8, the two-particle correlation being fully considered in Ref. 8.

The formation of electronic quantum dots at the juncture of three orthogonal quantum wells fabricated with twofold CEO (2CEO) was predicted by us.[7] Such quantum dots have been realized in the meantime,[9] and our calculations have been quantitatively confirmed.

The dielectric constants of the well and host materials are different, which causes image charge effects. Those were found to be of appreciable size for quantum wells.[10] For quantum wires and dots their impact was ignored until now.

We had shown in Ref. 7 that a deeper confinement potential leads to an increase of the exciton localization in CEO T-shaped quantum wires and 2CEO quantum dots in the (unstrained) $GaAs/Al_xGa_{1-x}As$ material system. In order to improve the relatively weak localization of carriers further, it seems reasonable to use strained material combinations, such as $In_xGa_{1-x}As/Al_xGa_{1-x}As$ with a larger difference in band gaps. At the juncture the strain *energy* will relax, and potentially change the strain *components* in such a way that an even more attractive potential develops. To the best of our knowledge, strained CEO structures have not been theoretically treated before. We will show that the situation is rather complex, and that the above idea can be exploited for QWR's but not for dots.

We note that a related system is a barrier–quantum-well–barrier layer sequence grown on the cleaved edge of a strained superlattice. Such a system was experimentally studied in Ref. 11, and theoretically discussed in Ref. 12. However, the intermediate barrier layer creates a topologically entirely different situation compared to T-shaped QWR's. The strain effect of the underlying superlattice on the CEO quantum well seems then to be negligibly small.[12]

II. IMAGE CHARGE EFFECTS

The difference between the dielectric constants of the well and barrier materials leads to image charge effects. The impact of image charges on two-dimensional excitons in quantum wells was treated in Ref. 8. For zero-dimensional excitons (analytical), solutions have been obtained so far only for spherical geometry.[13] In order to obtain the correct electrostatic potential $V(\mathbf{r})$ of a charge distribution $\rho(\mathbf{r})$, the Poisson equation is numerically solved with spatially varying dielectric constant, $\varepsilon(\mathbf{r})\Delta V(\mathbf{r})+\nabla V(\mathbf{r})\nabla\varepsilon(\mathbf{r})=-\rho(\mathbf{r})/\varepsilon_0$. At interfaces the solution shows that the tangential component of the electric field **E** and the normal component of the induction field **D** are continuous. To quantify the effect of images charges, in Fig. 1 we show the results for a GaAs/AlAs

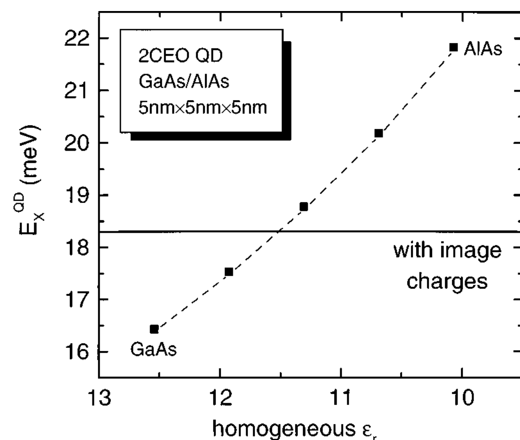

FIG. 1. Exciton binding energy in a $5\times5\times5$-nm^3 2CEO GaAs/AlAs quantum dot. The solid line (18.3 meV) represents the value obtained taking the spatial dependence of the dielectric constant properly into account. The squares (the dashed line is a guide to the eye) have been calculated by assuming various fixed homogeneous dielectric constants between the limiting values of GaAs and AlAs.

 © 1998 The American Physical Society

2CEO quantum dot where all QWL's are 5 nm thick. First, the exciton binding energy is calculated using the correct spatial dependence of $\varepsilon(\mathbf{r})$, i.e., including the image charges (solid line). The results for a *fixed homogeneous* dielectric constant, whose value was varied between the values of GaAs and AlAs, is shown by squares (dashed curve is guide to the eye). Compared to the calculation with constant $\varepsilon(\mathbf{r}) \equiv \varepsilon_{\mathrm{GaAs}}$ throughout the structure, the correct exciton binding energy is 2 meV, about 10%, larger.

III. STRAINED CEO QUANTUM WIRES

In a (two-dimensional) film the in-plane strain $\varepsilon_{\parallel}$ is given by the relative lattice mismatch $\varepsilon_{\parallel}=\varepsilon_0=(a_s-a_f)/a_f$, where a_s and a_f denote the unstrained lattice constants of the substrate and film bulk material, respectively. The strain $\varepsilon_{\perp}$ perpendicular to the film for an isotropic medium is given by $\varepsilon_{\perp}=-2\varepsilon_0\nu/(1-\nu)$, ν being the Poisson constant. For an anisotropic solid the ratio $\varepsilon_{\perp}/\varepsilon_0$ depends on the orientation. For the two relevant orientations in CEO QWR's and 2CEO dots, the (001) and (110) planes, well-known expressions for cubic semiconductors exist:[14,15]

$$\varepsilon_{\perp}^{001}=-\varepsilon_0\,\frac{2C_{12}}{C_{11}} \quad \text{and} \quad \varepsilon_{\perp}^{110}=-\varepsilon_0\,\frac{2C_{12}-C_0/2}{C_{11}+C_0/2},$$

where C_{ij} denote the elastic compliances, and $C_0=2C_{44}+C_{12}-C_{11}$ is the anisotropy index. The hydrostatic strain $\varepsilon_H=2\varepsilon_{\parallel}+\varepsilon_{\perp}$, that determines the shift of the conduction band, thus depends on the orientation. We note that for an isotropic solid, i.e., when $C_0=0$, the hydrostatic strain of a structure of arbitrary form in an infinite matrix is constant.[16] But since C_0 is positive for all common semiconductors, consequently $\varepsilon_H^{001}/\varepsilon_0<\varepsilon_H^{110}/\varepsilon_0$. The conduction-band (CB) edge of the strained film is given by $E_c=E_{c,0}+a_c\varepsilon_H$, where $E_{c,0}$ is the CB edge of the unstrained bulk material, and a_c is the hydrostatic CB deformation potential. Therefore the CB edge in the (110) QWL is generally higher in energy than in the (001) QWL (for compressive strain, $a_f>a_s$).

For T-shaped QWR's and dots, the strain distribution is calculated using continuum strain theory as outlined in Ref. 16. Boundary conditions at interfaces are realized by using virtual interface voxels. Strain calculations were also performed using the valence-force-field (VFF) model,[17,18] providing an atomic description. The compliance C_{44} in this *two-parameter* model is not an independent parameter, and is fixed to a slightly different value than that entering continuum strain theory. Hence the quantitative results of the VFF calculation, especially along $\langle 110\rangle$ (and $\langle 111\rangle$) directions, are slightly different from those based on the three parameter continuum model. The following numerical results are therefore based on continuum strain theory.

Generally at the T-shaped juncture, strain *energy* is relaxed. In Fig. 2(a) the CB edge of a symmetric $\mathrm{In_{0.2}Ga_{0.8}As/GaAs}$ T-shaped QWR ($d^{001}=d^{110}=5$ nm) is shown. The numerical values used in the calculations are given in Table I. Along the (110) QWL the hydrostatic strain partially relaxes at the junction to the (001) QWL, as compared to the strict (110) case far away from the junction (solid line). This effect creates an attractive potential for electrons. However, the lowest potential is found in the (001) QWL far away from the intersection (dashed line). In large structures, where the electron confinement energies are small compared to $E_c^{110}-E_c^{001}$, the carriers will therefore "flow out" from the intersection into the (001) QWL. In contrast, for small structures the confinement effects due to size quantization may be tuned in such a way that the difference in strain-induced shifts is compensated for and the attractive potential dip along the (110) QWL is utilized.

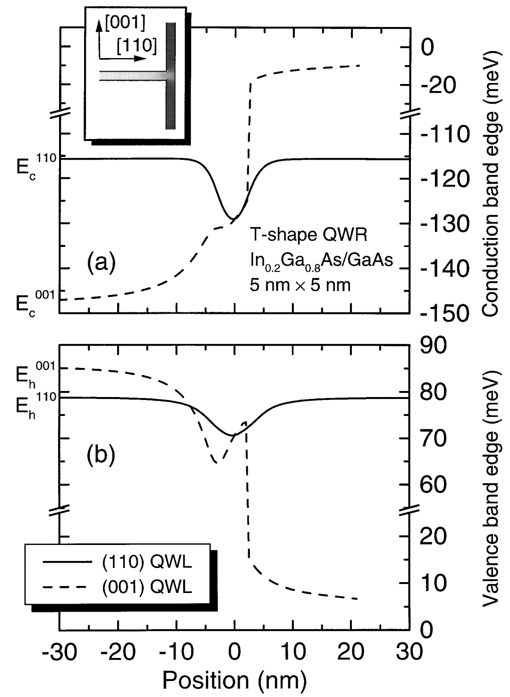

FIG. 2. (a) Conduction-band edge in a strained 5×5-nm^2 T-shaped $\mathrm{In_{0.2}Ga_{0.8}As/GaAs}$ QWR. Inset: Two-dimensional plot with indication of crystal directions. Solid line: line scan at the center of the (110) QWL in the [001] direction. Dashed line: line scan at the center of the (001) QWL in the [110] direction. (b) Valence-band edge. The zero position is in the center of the intersection of the two quantum wells. The band edges of unstrained GaAs are at $E_c=E_h=0$.

The additional electron confinement energy $E_{\mathrm{conf},e}$ must fulfill both the conditions $E_e^{\mathrm{QWR}}<E_c^{001}+E_{\mathrm{conf},e}^{001}$ and $E_e^{\mathrm{QWR}}<E_c^{110}+E_{\mathrm{conf},e}^{110}$ to ensure the localization of electrons. In order to push up the electron level in the (001) QWL, one may tend to choose a smaller value for d^{001} than for d^{110}, creating an asymmetric QWR.

Another possibility to shift the band edge in the (001) quantum well is the use of different indium contents in the (001) and (110) parts. In order to increase the CB edge of the (001) QWL, a lower indium content is required. This, however, would reduce the depth of the attractive potential in the (110) QWL.

The valence-band edge, calculated in a six-band $\mathbf{k}\cdot\mathbf{p}$ scheme,[16,20] is higher in the (001) QWL than in the (110) QWL [Fig. 2(b)]. Therefore, holes in large structures will tend to diffuse into the (001) QWL. Due to the potential barrier at the intersection, the movement from the (110) QWL into the (001) QWL will be inhibited at low temperatures. For sufficiently small structures the holes will localize in the (110) QWL because of the larger mass in the [110]

TABLE I. Low-temperature material parameters of GaAs and $In_{0.2}Ga_{0.8}As$ used in the calculations: lattice constant a_0, band gap E_g, average valence-band position $E_{v,\mathrm{av}}$ (Ref. 14), spin-orbit splitting Δ_0, elastic constants C_{11}, C_{12}, and C_{44}, hydrostatic deformation potentials (Ref. 14) for the band gap a and the conduction band a_c, shear deformation potentials b [110] and d [111], relative dielectric constant ε_r, electron mass m_e, and Luttinger parameters γ_1, γ_2, and γ_3 (all parameters have been taken from Ref. 19 unless indicated otherwise).

	GaAs	$In_{0.2}Ga_{0.8}As$
a_0 (nm)	0.565 33	0.5734
E_g (eV)	1.519	1.222
$E_{v,\mathrm{av}}$ (eV)	−6.92	−6.87
Δ_0 (eV)	0.34	0.346
C_{11} (10^{10} Pa)	12.11	11.35
C_{12} (10^{10} Pa)	5.48	5.29
C_{44} (10^{10} Pa)	6.04	5.62
a (eV)	−8.33	−7.88
a_c (eV)	−7.17	−6.75
b (eV)	−1.9	−1.83
d (eV)	−4.23	−4.0
ε_r	12.53	13.36
m_e	0.067	0.059
γ_1	6.85	9.42
γ_2	2.1	3.36
γ_3	2.9	4.18

direction. For the numerical modeling, anisotropic hole masses $m_{\mathrm{hh}}^{001}=1/(\gamma_1-2\gamma_2)$ and $m_{\mathrm{hh}}^{110}=2/(2\gamma_1-\gamma_2-3\gamma_3)$ (Ref. 8) have been used.

In the single-particle approximation the strained T-shaped QWR thus represents a type-II situation, i.e., the electron may be confined at the intersection, but the hole is delocalized from that region. Now the Coulomb interaction is taken into account additionally. This is done in the Hartree approximation,[21] that was also used in Ref. 7. The excitonic wave function is approximated as the product of an electron and a hole wave function. Each single-particle wave function is calculated self-consistently in the Coulomb potential of the oppositely charged particle. In this approximation the two-particle character of the wave function that was discussed for unstrained T-shaped QWR's in Ref. 8 is neglected. For the energy levels a good approximation is obtained.

In Fig. 3 the electron and heavy-hole orbitals of the excitonic wave function in a 4×5-nm^2 $In_{0.2}Ga_{0.8}As$/GaAs quantum wire are shown together with two-dimensional plots of the electron and heavy-hole probability densities. The recombination and localization energies of excitons in the (001) and (110) quantum wells and in the T-shaped QWR formed at their juncture is shown in Fig. 4 for constant $d^{001}=4$ nm and varying d^{110}. For $d^{110}>4$ nm, bound states are found for the QWR exciton with a maximum localization energy of 10 meV.

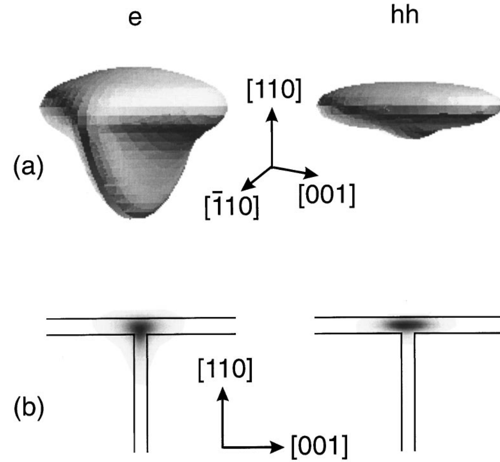

FIG. 3. (a) Three-dimensional view of the electron and (heavy) hole parts of the excitonic wave function in a 4×5-nm^2 T-shaped $In_{0.2}Ga_{0.8}As$/GaAs QWR; the orbitals correspond to 70% probability inside. (b) Cross section through the electron and hole orbitals in their center along the [$\bar{1}$10] direction.

IV. STRAINED 2CEO QUANTUM DOTS

At the juncture of three QWL's, the strain *energy* is further relaxed. The conduction-band edge at the juncture of three (001), (110) and (1-10) $In_{0.2}Ga_{0.8}As$/GaAs quantum wells is shown in Fig. 5. In the (001) cross section [Figs. 5(a) and 5(b)], the juncture has the highest potential. In the (1-10) QWL plane [Figs. 5(c) and 5(d)] the potential exhibits a small drop (about 5 meV) along the [110] direction on top of the (110) QWL; the lowest potential, however, is present at the juncture of the (001) and the (1-10) quantum wells. Both electrons and holes are repelled from the juncture, and the effect of (compressive) strain generally counteracts the localization of carriers in a 2CEO quantum dot. If the strain is small, and again an asymmetric [thin (001) quantum well]

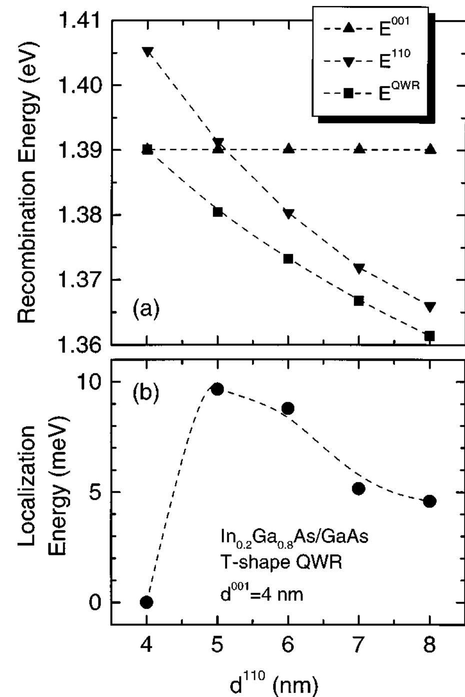

FIG. 4. (a) Exciton recombination energy in strained $In_{0.2}Ga_{0.8}As$/GaAs structures: 4-nm (001) QWL, (110) QWL with varying thickness (d^{110}) and in 4-nm$\times d^{110}$ T-shaped QWR. (b) Localization energy of a QWR exciton with respect to the minimum of QWL energies. For $d^{001}=d^{110}=4$ nm, the exciton is no longer localized.

FIG. 5. Geometry [(a) and (c)] and conduction band edge [(b) and (d) (color)] in meV ($E_c^{\mathrm{GaAs}}=0$) of a 2CEO $\mathrm{In_{0.2}Ga_{0.8}As/GaAs}$ quantum dot; $d^{001}=4$ nm, and $d^{110}=d^{1-10}=6$ nm. (a) and (b) show the intersection through the center of the (001) quantum well, and (c) and (d) the intersection through the center of the (1–10) quantum well. Dashed white lines in (a) and (c) denote contours of hidden quantum wells. The conduction-band edge in (b) has been masked to show only the value in the $\mathrm{In}_x\mathrm{Ga}_{1-x}\mathrm{As}$.

geometry is chosen, a bound state may still form when the kinetic quantization effects overcome the repulsive potential due to strain effects. If the strain is sufficiently large, it dominates, and no bound states exist for 2CEO dots. In a numerical example for a $4\times6\times6$-nm^3 $\mathrm{In_{0.2}Ga_{0.8}As/GaAs}$ dot, we find still weakly (<3 meV) bound electrons. However, even inclusion of Coulomb interaction does not lead, to the formation of a direct exciton in this case.

V. IMPACT OF STRAIN ON EPITAXIAL GROWTH

The previous discussion has shown that the impact of strain on the *electronic properties* of CEO nanostructures does not provide a straightforward improvement of carrier confinement compared to unstrained structures. However, perfectly *flat* QWL geometry has been assumed.

Strain, however, could also impact the *growth morphology*. Locally thicker structures could form on top of the cleaved edge of the original QWL's due to strain relaxation during growth. In this case carrier localization is increased. To elucidate this point, the change of the (110) surface unit cell area of an $\mathrm{In}_x\mathrm{Ga}_{1-x}\mathrm{As}$ layer grown on the cleaved edge of an $\mathrm{In}_x\mathrm{Ga}_{1-x}\mathrm{As/GaAs}$ quantum well is shown in Fig. 6. Along the [1-10] direction (wire direction), the $\mathrm{In}_x\mathrm{Ga}_{1-x}\mathrm{As}$

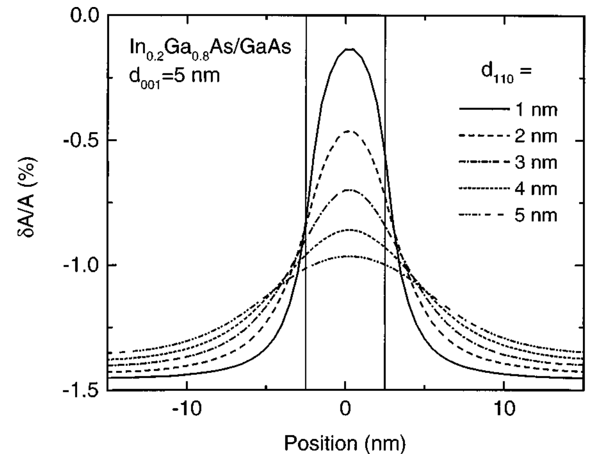

FIG. 6. Relative change of the surface unit-cell area of an $\mathrm{In_{0.2}Ga_{0.8}As}$ (110) surface grown on top of the cleaved edge of a 5-nm-thick (001) $\mathrm{In_{0.2}Ga_{0.8}As/GaAs}$ QWL (indicated by vertical solid lines). The position along [001] is counted from the center of the (001) QWL. Different curves correspond to different thicknesses of a (flat) $\mathrm{In}_x\mathrm{Ga}_{1-x}\mathrm{As}$ layer on the (110) surface.

lattice constant is compressed to that of GaAs. Along the [001] direction the expansion of the (001) QWL introduces tensile strain in the $In_xGa_{1-x}As$. The resulting surface unit cell area directly above the (001) QWL thus exhibits values closer to that of bulk $In_xGa_{1-x}As$ than in any other part of the (110) QWL. Thus the (110) film strain can achieve a reduction of strain energy if material diffuses to the region above the (001) QWL. Of course, this mechanism depends on sufficient diffusion length under the given growth conditions. A similar argument holds for the surface unit cell area in the (1-10) layer on top of the T-shaped QWR in the case of the growth of 2CEO dots. Similar modification of surface strain and impact on growth kinetics has been modeled for and experimentally observed in vertically aligned stacks of self-ordered quantum dots.[22–24]

VI. CONCLUSION

The properties of compressively strained CEO quantum wires and dots are theoretically predicted in the framework of effective-mass theory including excitonic and image charge effects. As the model material, an $In_{0.2}Ga_{0.8}As/GaAs$ system was used. A bound state is predicted in *asymmetric* QWR's at the juncture of (001) and (110) quantum wells. The (110) quantum-well width generally has to be chosen larger than that of the (001) quantum well. Localization energies of up to 10 meV are expected. In compressively strained 2CEO dots the strain effects generally counteract carrier localization, and can prohibit the formation of bound states. The strain-induced modification of growth morphology has been discussed.

ACKNOWLEDGMENTS

We are indebted to A. Schliwa for assistance with the numerical calculations, and to V. A. Shchukin for helpful discussions. This work was funded by Deutsche Forschungsgemeinschaft in the framework of Sfb 296.

[1] L. Pfeiffer, K. W. West, H. L. Störmer, J. P. Eisenstein, K. W. Baldwin, D. Gershoni, and J. Spector, Appl. Phys. Lett. **56**, 1697 (1990).

[2] A. R. Goñi, L. N. Pfeiffer, K. W. West, A. Pinczuk, H. U. Baranger, and H. L. Störmer, Appl. Phys. Lett. **61**, 1956 (1992).

[3] T. Someya, H. Akiyama, and H. Sakaki, Phys. Rev. Lett. **74**, 3664 (1995).

[4] A. A. Kiselev and U. Rössler, Semicond. Sci. Technol. **11**, 203 (1996).

[5] L. Pfeiffer, H. Baranger, D. Gershoni, K. Smith, W. Wegscheider, in *Low Dimensional Structures Prepared by Epitaxial Growth or Regrowth on Patterned Substrates*, edited by K. Eberl, P. M. Petroff, and P. Demeester (Kluwer, Dordrecht, 1995), p. 93.

[6] W. Langbein, H. Gislason, and J. M. Hvam, Phys. Rev. B **54**, 14 595 (1996).

[7] M. Grundmann and D. Bimberg, Phys. Rev. B **55**, 4054 (1997).

[8] S. Glutsch, F. Bechstedt, W. Wegscheider, and G. Schedelbeck, Phys. Rev. B **56**, 4108 (1997).

[9] W. Wegscheider, G. Schedelbeck, G. Abstreiter, M. Rother, and M. Bichler, Phys. Rev. Lett. **79**, 1917 (1997).

[10] D. B. Tran Thoai, R. Zimmermann, M. Grundmann, and D. Bimberg, Phys. Rev. B **42**, 5906 (1990).

[11] D. Gershoni, J. S. Weiner, S. N. G. Chu, G. A. Baraff, J. M. Vandenberg, L. N. Pfeiffer, K. West, R. A. Logan, and T. Tanbun-Ek, Phys. Rev. Lett. **65**, 1631 (1990).

[12] C. Priester and S. J. Sferco, Phys. Rev. B **55**, 6693 (1997).

[13] L. E. Brus, J. Chem. Phys. **80**, 4403 (1984).

[14] Ch. G. Van der Walle, Phys. Rev. B **39**, 1871 (1989).

[15] A. Segmüller, I. C. Noyan, and V. S. Speriosu, Prog. Cryst. Growth Charact. **18**, 21 (1989).

[16] M. Grundmann, O. Stier, and D. Bimberg, Phys. Rev. B **52**, 11 969 (1995).

[17] P. N. Keating, Phys. Rev. **145**, 637 (1966).

[18] Since the magnitude of the nonlinear terms in Ref. 17 cannot be justified, we have used the linearized version as proposed by E. O. Kane, Phys. Rev. B **31**, 7865 (1985).

[19] *Semiconductors Physics of Group IV Elements and III–V Compounds*, edited by O. Madelung, M. Schulz, and H. Weiss, Landolt-Börnstein, New Series, Group III, Vol. 17, Pt. a (Springer, Berlin, 1982).

[20] Y. Zhang, Phys. Rev. B **49**, 14 352 (1994).

[21] L. Bányai and S. W. Koch, *Semiconductor Quantum Dots*, World Scientific Series on Atomic, Molecular and Optical Properties Vol. 2 (World Scientific, Singapore, 1993).

[22] M. Grundmann, R. Heitz, N. Ledentsov, O. Stier, D. Bimberg, V. M. Ustinov, P. S. Kop'ev, Zh. I. Alferov, S. S. Ruvimov, P. Werner, U. Gösele, and J. Heydenreich, Superlattices Microstruct. **19**, 81 (1996).

[23] N. N. Ledentsov, V. A. Shchukin, M. Grundmann, N. Kirstaedter, J. Böhrer, O. Schmidt, D. Bimberg, V. M. Ustinov, A. Yu. Egorov, A. E. Zhukov, P. S. Kop'ev, S. V. Zaitsev, N. Yu. Gordeev, Zh. I. Alferov, A. I. Borovkov, A. O. Kosogov, S. S. Ruvimov, P. Werner, U. Gösele, and J. Heydenreich, Phys. Rev. B **54**, 8743 (1996).

[24] Q. Xie, A. Madhukar, P. Chen, and N. Kobayashi, Phys. Rev. Lett. **75**, 2542 (1995).